Wireless Pers Commun (2012) 67:783–801
DOI 10.1007/s11277-011-0409-1

Low Complexity Time-Concatenated Turbo Equalization for Block Transmission without Guard Interval: Part 2—Application to SC-FDMA

Hui Zhou · Khoirul Anwar · Tad Matsumoto

Published online: 25 September 2011

Abstract The primary objective of this paper is to apply the CHATUE algorithm, presented in the Part-1 paper of this article, to multi-user Single Carrier Frequency Division Multiple Access (SC-FDMA) Systems. The CHATUE algorithm connects turbo equalizers neighboring in time in the absence of Cyclic Prefix or Guard Interval, where the latest version of the reduced complexity equalization technique, Frequency Domain Soft Cancellation Minimum Mean Square Error turbo equalization is utilized not only to mitigate the inter-carrier interference but also to eliminate the inter-block interferences from the neighboring blocks. Furthermore, doped accumulator is combined with our proposed CHATUE-SC-FDMA system. Extrinsic Information Transfer analysis is used to demonstrate the improvement in convergence property as well as to analyze the bit error rate threshold. This paper provides in detail the time-concatenated turbo equalization algorithm for SC-FDMA, referred to as CHATUE-SC-FDMA, and evaluates its performances. When deriving the algorithm, we also propose, without imposing significant performance degradation, an approximation technique to eliminate the necessity of the covariance matrix inversion.

Keywords SC-FDMA · CHATUE · Cyclic Prefix · DA · EXIT chart

This research has been supported in part by SANYO Electric Co. Ltd, Kinki Mobile Communications Center, and in part by Chubu Electric Co. Ltd.

H. Zhou (✉) · K. Anwar · T. Matsumoto
School of Information Science, Japan Advanced Institute of Science and Technology,
1-1 Asahidai, Nomi, Ishikawa 923-1292, Japan
e-mail: hui-z@jaist.ac.jp

K. Anwar
e-mail: anwar-k@jaist.ac.jp

T. Matsumoto
e-mail: matumoto@jaist.ac.jp; tadashi.matsumoto@ee.oulu.fi

T. Matsumoto
Center of Wiereless Communications (CWC), University of Oulu, 90014 Oulu, Finland

1 Introduction

The Long-Term Evolution (LTE) project in the framework of the Evolved-Universal Terrestrial Radio Access Network (E-UTRAN) has adopted Orthogonal Frequency Division Multiplexing (OFDM) for downlink transmission in next generation wireless cellular communications systems (4G) [1], because of its flexibility in satisfying each user's Quality-of-Service (QoS) requirements. On the other hand, Single Carrier Frequency Division Multiple Access (SC-FDMA) [2] has been adopted as the uplink transmission technique because of its lower Peak-to-Average Power Ratio (PAPR) than OFDM, and hence is well suited for power efficient transmission at the mobile terminals. As in OFDM, SC-FDMA exhibits robustness against frequency-selectivity with the aid of a low complexity sub-optimal frequency domain turbo equalization technique, of which technological bases have been presented in the Part-1 paper of this article [3].

The traditional SC-FDMA uses cyclic prefix (CP) as a guard interval (GI) to avoid the Inter-Block Interference (IBI), resulting from fading multi-path propagation. With the CP-Transmission, the channel matrix has a circulant structure, and hence is effective in significantly reducing the computational complexity for signal detection, such as [4,5], where [4] applies the decision feedback equalization (DFE) to SC-FDMA systems; a frequency domain DFE algorithm is presented in [5], which avoids the necessity to calculate the inverse matrices, required to obtain feedback and feed-forward filters. However, CP transmission systems incur decrease in power and spectral efficiencies. Furthermore, if the time duration of the CP is shorter than the channel impulse response, the overall system performance is severely degraded by the interferences. As a result, despite the fact that SC-FDMA with CP/GI has advantages [2,6] such as low PAPR, robustness against carrier frequency offset, and low computational complexity, it has also disadvantages such as loss in the power and spectral efficiencies due to the necessity of the CP transmission.

The original version of the technique proposed in this article is partly presented in [7]. This paper is a sister paper of its Part-1 article [3], and the primary objective of this paper is to apply the major results of the Part-1 article to SC-FDMA systems.

Despite the volume of the publications on no GI transmission techniques for OFDM and single carrier block transmission, only a few have been published for SC-FDMA-GI/CP-free transmission. In-depth literature survey and performance comparison for GI-free transmission techniques are provided in the Part-1 paper for OFDM and single carrier block transmission. For multiuser SC-FDMA systems, a blind eigen-analysis based beamforming algorithm has been proposed in [8] to eliminate the self-interference caused by insufficient CP.

In the Part-1 paper, the idea of connecting the neighboring equalization blocks in time has been proposed. This concept is referred to as CHained TUrbo Equalization (CHATUE), with which the necessity of transmitting GI can well be avoided while eliminating the Inter-Block Interference (IBI) components through the exchange of Log-Likelihood Ratio (LLR) between the neighboring blocks. To collect the total signal energy, sampling of the received signal has to continue until the end of IBI due to the last symbol in the current block, which overlaps the head of the following block. The latest version of the reduced complexity equalization technique-Frequency Domain Soft Cancellation MMSE (FD/SC-MMSE) [9] turbo equalization is utilized in the Part-1 paper, which can effectively eliminate the interference components without requiring heavy computational burden.

In this paper, we propose a novel frequency domain turbo equalization technique for SC-FDMA systems without CP, by making several relevant modifications on the CHATUE algorithm [3] so that it can be well adjusted to the SC-FDMA sub-carrier mapping.

Furthermore, we utilized the Doped Accumulator (DA) in our proposed system to further improve the performance.

Results of the convergence property and BER performance evaluations are presented in this paper for the proposed CHATUE-SC-FDMA as well as for the traditional OFDM with CP transmission, referred to as CP-SC-FDMA. The simulation results show that BER performance versus per-bit energy-to-noise spectral density ratio with the proposed CHATUE-SC-FDMA and CP-SC-FDMA techniques are almost identical. This indicates that by using the proposed CHATUE-SC-FDMA technique, the loss in spectrum efficiency due to the CP transmission can totally be recovered. Furthermore, by using the time duration, made available by eliminating the CP/GI, we can employ even lower rate code, and the use of the lower rate code can enhance the power efficiency of the system, if the frame structure should not be changed due to some practical reason (in the other words, if spectrum efficiency has to be the same as the traditional CP-SC-FDMA).

This paper is organized as follows; Sect. 2 shows the system model as well as mathematical derivations of the equations related to the model. Section 3 describes the CHATUE algorithm for SC-FDMA. Quantitative complexity evaluation is also provided in Sect. 3. The Sect. 4 presents Extrinsic Information Transfer (EXIT) chart to analyse the convergence behavior of the proposed system. The performance comparison against traditional SC-FDMA with CP transmission as well as against another CP-free block transmission technique, CP compensation [10], is presented in Sect. 5. Conclusions are drawn in Sect. 6.

In this paper, the bold mathematical symbols indicate the matrix. Past and future blocks are indicated by $\bullet'$, $\bullet''$. respectively. A diagonal matrix constructed by taking the diagonal components of the argument matrix is denoted by diag($\bullet$), Hermitian and Transpose of a matrix are indicated by $\bullet^H$, $\bullet^T$, respectively. $\mathbf{E}(\bullet)$ stands for the expectation of its argument. $\hat{\bullet}$ indicates the estimate of a variable. $tr(\bullet)$ denotes trace product and $\mathbf{I}_K$ indicates a $K \times K$ identity matrix. Furthermore, L_e, L_a and L_p denote the extrinsic, *a priori* and *a posteriori* LLRs, respectively.

2 System Model

In this paper we consider a multi-user Single-Input Single-Output SC-FDMA system. Basic structure of the SC-FDMA transceiver this paper assumes is shown in Fig. 1. The information bits are encoded ($\mathbf{C}_{i,t}$), random interleaved ($\mathbf{\Pi}_{i,t}$), doped-accumulated and modulated to obtain the signal vectors $\mathbf{s}'_{i,t-1}$, $\mathbf{s}_{i,t}$, and $\mathbf{s}''_{i,t+1}$, where i is the user index, and t stands for the current block. After performing the sub-carrier mapping, which is represented by the mapping matrix $\mathbf{D}_i$, the frequency-domain signal is converted back to the time-domain, and transmitted over the frequency-selective block quasi-static multi-path Rayleigh fading channels.

Multiplying by the matrix $\mathbf{J}$, the equivalent block-wise Toeplitz current channel matrix $\mathbf{H}_{i,t}$ can be converted into a circulant matrix, $\mathbf{J}\mathbf{H}_{i,t}$. The received composite signal can be expressed as

$$\mathbf{r}_t = \sum_{i=1}^{I} \mathbf{r}_{i,t} + \mathbf{J}\mathbf{n}, \tag{1}$$

where

$$\mathbf{r}_{i,t} = \mathbf{J}\mathbf{H}_{i,t}\mathbf{F}_M^H\mathbf{D}_i\mathbf{F}_K\mathbf{s}_{i,t} + \mathbf{J}\mathbf{H}'_{i,t-1}\mathbf{F}_M^H\mathbf{D}_i\mathbf{F}_K\mathbf{s}'_{i,t-1} + \mathbf{J}\mathbf{H}''_{i,t+1}\mathbf{F}_M^H\mathbf{D}_i\mathbf{F}_K\mathbf{s}''_{i,t+1} \tag{2}$$

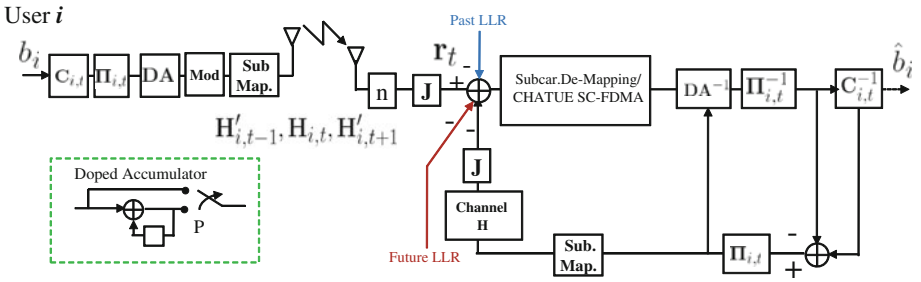

Fig. 1 The proposed transceiver structure without CP in multiuser SC-FDMA

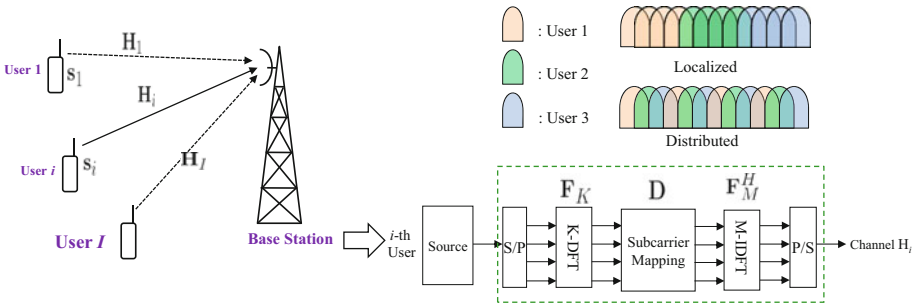

Fig. 2 SC-FDMA's sub-carrier mapping

with I denoting the number of users. $\mathbf{n}$ is a zero mean complex white Gaussian noise vector with variance σ_n^2.

Note that the equivalent signal vectors transmitted in the past, current and future blocks $\mathbf{s}'_{i,t-1}$, $\mathbf{s}_{i,t}$, $\mathbf{s}''_{i,t+1}$, and their corresponding equivalent block-wise channel matrices $\mathbf{H}'_{i,t-1}$, $\mathbf{H}_{i,t}$, $\mathbf{H}''_{i,t+1}$ as well as the structure of matrix $\mathbf{J}$ are detailed in Appendix.

The SC-FDMA system assumed in this paper employs a frequency bin allocation matrix $\mathbf{D}_i$, where the dimensionality of $\mathbf{D}_i$ depends on each user's Quality of Service (QoS) requirement. As shown in Fig. 2, $\mathbf{D}_i$ is a $M \times K$ matrix, i.e. for the ith user, the κth sub-carrier component of the K-point Discrete Fourier Transform (DFT) is mapped to the mth sub-carrier of the M-point DFT, where $0 \leq \kappa \leq K-1, 0 \leq m \leq M-1$.

For localized sub-carrier mapping,

$$\mathbf{D}_i = \begin{cases} 1 & m = R_u \cdot M + \kappa \\ 0 & \text{otherwise} \end{cases} \tag{3}$$

and for distributed sub-carrier mapping,

$$\mathbf{D}_i = \begin{cases} 1 & m = R_u + \frac{K}{M} \cdot \kappa \\ 0 & \text{otherwise} \end{cases} \tag{4}$$

with R_u indicating the resource unit allocation [4], which is subjected to $0 \leq R_u \leq \frac{K}{M} - 1$.

It is assumed that $\mathbf{D}_i$ is the same over the past, current, and future blocks. Since $\mathbf{D}_i$ is an orthogonal matrix, $\mathbf{D}_i^T \mathbf{D}_i = \mathbf{I}_K$. The M-point DFT matrix $\mathbf{F}_M$ is larger in size than the K-point DFT matrix $\mathbf{F}_K$. It is well known that the DFT matrix $\mathbf{F}_M$ is a unitary matrix, i,e. $\mathbf{F}_M \mathbf{F}_M^H = \mathbf{F}_M^H \mathbf{F}_M = \mathbf{I}_M$.

In this paper, we define the system-signal to noise ratio (SNR) by

$$\mathrm{SNR} = \frac{\sum_{i=1}^{I} P_i}{B N_0} \tag{5}$$

with P_i, B, N_0 denoting the power allocated to the ith user, total bandwidth, and noise power spectral density, respectively.

3 Proposed CHATUE-SC-FDMA Algorithm

3.1 Soft Cancellation

We utilize the soft estimates of the past, current, and future blocks $\hat{\mathbf{s}'}_{t-1}$, $\hat{\mathbf{s}}_t$ and $\hat{\mathbf{s}''}_{t+1}$, respectively, to construct a soft replica of the receive signal as

$$\begin{aligned}\hat{\mathbf{r}}_t = &\sum_{i=1}^{I} \mathbf{J}\mathbf{H}_{i,t}\mathbf{F}_M^H\mathbf{D}_i\mathbf{F}_K\hat{\mathbf{s}}_{i,t} + \sum_{i=1}^{I} \mathbf{J}\mathbf{H}'_{i,t-1}\mathbf{F}_M^H\mathbf{D}_i\mathbf{F}_K\hat{\mathbf{s}}'_{i,t-1} \\ &+ \sum_{i=1}^{I} \mathbf{J}\mathbf{H}''_{i,t+1}\mathbf{F}_M^H\mathbf{D}_i\mathbf{F}_K\hat{\mathbf{s}}''_{i,t+1}\end{aligned} \tag{6}$$

It is assumed that the channel matrices and the allocation matrices are known to the receiver. The soft estimates of the kth symbol in the current, past, and future blocks for the ith user are given by

$$\hat{s}_{i,t}(k) = \mathrm{E}[s_{i,t}(k)|L_{e,C_i^{-1}}] = \tanh\left\{L_{e,C_i^{-1}}[s_{i,t}(k)]/2\right\}, \tag{7}$$

$$\hat{s}'_{i,t-1}(k) = \mathrm{E}[s'_{i,t-1}(k)|L'_{p,C_{i,t-1}^{-1}}] = \tanh\left\{L'_{p,C_{i,t-1}^{-1}}[s'_{i,t-1}(k)]/2\right\}, \tag{8}$$

and

$$\hat{s}''_{i,t+1}(k) = \mathrm{E}[s''_{i,t+1}(k)|L''_{p,C_{i,t+1}^{-1}}] = \tanh\left\{L''_{p,C_{i,t+1}^{-1}}[s''_{i,t+1}(k)]/2\right\}, \tag{9}$$

when Binary Phase Shift Keying (BPSK) modulation is assumed. It should be noted that in the iterations between the equalizers, referred to as vertical iterations, the *a posteriori* LLR of the decoder from the past and future blocks, $L'_{p,C_{i,t-1}^{-1}}$ and $L''_{p,C_{i,t+1}^{-1}}$, respectively, are exchanged of as shown in Fig. 3. We, then, perform Soft Cancellation (SC) of ICI and IBI components, of which residual is given by

$$\tilde{\mathbf{r}}_t = \mathbf{r}_t - \hat{\mathbf{r}}_t. \tag{10}$$

The residual ICI and IBI components can be further suppressed by Minimum Mean Square Error (MMSE) algorithm as shown in Appendix. By performing the sub-carrier de-mapping, the ith users' signals are separated as

$$\tilde{\mathbf{r}}_{i,t} = \mathbf{F}_K^H\mathbf{D}_i^T\mathbf{F}_M\tilde{\mathbf{r}}_t = \mathbf{F}_K^H\mathbf{D}_i^T\mathbf{F}_M\mathbf{J}\mathbf{H}_{i,t}\mathbf{F}_M^H\mathbf{D}_i\mathbf{F}_K(\mathbf{s}_{i,t} - \hat{\mathbf{s}}_{i,t}) + \mathrm{IBI}, \tag{11}$$

$$\mathbf{F}_K^H\mathbf{D}_i^T\mathbf{F}_M\mathbf{J}\mathbf{H}_{i,t}\mathbf{F}_M^H\mathbf{D}_i\mathbf{F}_K(\mathbf{s}_{i,t} - \hat{\mathbf{s}}_{i,t}) = \bar{\mathbf{H}}_{i,t}(\mathbf{s}_{i,t} - \hat{\mathbf{s}}_{i,t}), \tag{12}$$

where, as mentioned before, $\mathbf{J}\mathbf{H}_{i,t}$ is a circulant matrix, and hence

$$\mathbf{\Phi}_{i,t} = \mathbf{D}_i^T\mathbf{F}_M\mathbf{J}\mathbf{H}_{i,t}\mathbf{F}_M^H\mathbf{D}_i \tag{13}$$

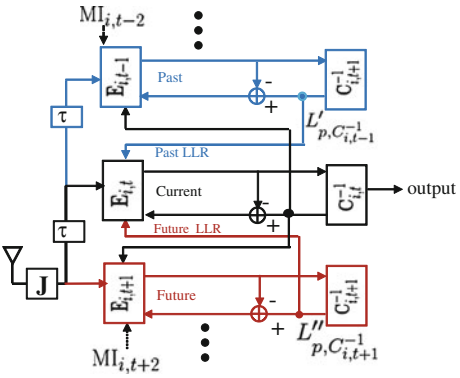

Fig. 3 Chained turbo equalization, where $\mathbf{E}_{i,t}$ and $\mathbf{C}_{i,t}^{-1}$ stand for the FD-SC/MMSE equalizer and BCJR decoder, respectively, and the mutual information from the $(t-2)$th and $(t+2)$th blocks, $\mathrm{MI}_{i,t-2}$ and $\mathrm{MI}_{i,t+2}$, are set at 0

becomes a diagonal matrix, since the sub-carrier mapping matrix $\mathbf{D}_i$ does not change in the frequency domain structure of the channel matrix. Finally, the equivalent channel matrix $\bar{\mathbf{H}}_{i,t}$ is found to be a circulant matrix, and hence we can make use of the beneficial points of the FD/SC-MMSE equalization algorithm.

After soft cancellation, the restoral term for the kth symbol is added, as

$$\tilde{s}(k)_{i,t} = \mathbf{r}_{i,t} - \hat{\mathbf{r}}_{i,t} + \bar{\mathbf{h}}(k)_{i,t}\hat{s}(k)_{i,t} = \tilde{\mathbf{r}}_{i,t} + \bar{\mathbf{h}}(k)_{i,t}\hat{s}(k)_{i,t}, \tag{14}$$

where $\bar{\mathbf{h}}(k)_{i,k}$ denotes the kth column vector of the equivalent current channel matrix $\bar{\mathbf{H}}_{i,t}$.

3.2 Equalizer Output

The block-wise equalization result is given in the form of vector $\mathbf{z}_{i,t}$, as

$$\begin{aligned}\mathbf{z}_{i,t} =& (\mathbf{I}_k + \mathbf{\Gamma}_{i,t}\mathbf{S}_{i,t})^{-1}\left[\mathbf{\Gamma}_{i,t}\hat{\mathbf{s}}_{i,t} + \mathbf{F}_K^H\mathbf{\Phi}_{i,t}^H\mathbf{F}_K\mathbf{\Sigma}_{i,t}^{-1}\tilde{\mathbf{r}}_{i,t}\right] \\ =& (\mathbf{I}_k + \mathbf{\Gamma}_{i,t}\mathbf{S}_{i,t})^{-1}\left[\mathbf{\Gamma}_{i,t}\hat{\mathbf{s}}_{i,t} + \mathbf{F}_K^H\mathbf{\Phi}_{i,t}^H\mathbf{X}^{-1}\mathbf{F}_K\tilde{\mathbf{r}_{i,t}}\right] \in C^{K\times 1},\end{aligned} \tag{15}$$

where the $\mathbf{\Gamma}_{i,t}$ can be expressed as

$$\begin{aligned}\mathbf{\Gamma}_{i,t} &= \mathrm{diag}\left[\bar{\mathbf{H}}_{i,t}^H\mathbf{\Sigma}_{i,t}^{-1}\bar{\mathbf{H}}_{i,t}\right] \\ &= \mathrm{diag}\left[\mathbf{F}_K^H\mathbf{\Phi}_{i,t}^H\mathbf{F}_K\mathbf{\Sigma}_{i,t}^{-1}\mathbf{F}_K^H\mathbf{\Phi}_{i,t}\mathbf{F}_K\right] \\ &= \mathrm{diag}\left[\mathbf{F}_K^H\mathbf{\Phi}_{i,t}^H\mathbf{X}^{-1}\mathbf{\Phi}_{i,t}\mathbf{F}_K\right] \in C^{K\times K}\end{aligned} \tag{16}$$

with $\mathbf{X}$ being the frequency domain covariance matrices given by

$$\begin{aligned}\mathbf{X} = \mathbf{F_K}\Sigma_{\mathbf{i,t}}\mathbf{F_K}^H =& \mathbf{\Phi}_{i,t}\mathbf{F}_K\mathbf{\Lambda}_{i,t}\mathbf{F}_K^H\mathbf{\Phi}_{i,t}^H + \mathbf{F}_K\sigma_i^2\mathbf{D}_i^T\mathbf{J}\mathbf{J}^H\mathbf{D}_i\mathbf{F}_K^H \\ &+ \mathbf{F}_K\bar{\mathbf{H}}'_{i,t-1}\mathbf{\Lambda}'_{i,t-1}\bar{\mathbf{H}}'^H_{i,t-1}\mathbf{F}_K^H \\ &+ \mathbf{F}_K\bar{\mathbf{H}}''_{i,t+1}\mathbf{\Lambda}''_{i,t+1}\bar{\mathbf{H}}''^H_{i,t+1}\mathbf{F}_K^H \in C^{K\times K}\end{aligned} \tag{17}$$

and

$$\sigma_i^2 = \frac{K}{M}\sigma_n^2. \tag{18}$$

for the ith user.

We assume that the MMSE filter output $\mathbf{z}_{i,t}$ can be approximated as an equivalent Gaussian channel output having input $\mathbf{s}_{i,t}$, as

$$\mathbf{z}_{i,t} = \mu \mathbf{s}_{i,t} + \nu, \tag{19}$$

where

$$\mu = \mathrm{E}[\mathbf{z}_{i,t} \cdot \mathbf{s}_{i,t}*] = \frac{1}{K}\mathrm{tr}\left[\mathbf{\Gamma}_{i,t}(\mathbf{I}_K + \mathbf{\Gamma}_{i,t}\mathbf{S}_{i,t})^{-1}\right], \tag{20}$$

with $\mathrm{E}[|\mathbf{s}_{i,t}|^2] = 1$ for BPSK modulation and ν being equivalent noise vector with variance given by

$$\sigma_\nu^2 = \mu(1-\mu). \tag{21}$$

Now, we can convert the MMSE filter output into an extrinsic LLR, as

$$\mathbf{L}_{a,E} = \ln \frac{Pr\left(z|s_{i,t}^{[k]} = +1\right)}{Pr\left(z|s_{i,t}^{[k]} = -1\right)} = \frac{4\Re(\mathbf{z})}{1-\mu}, \tag{22}$$

where $\Re(\mathbf{z})$ denotes the real part of the complex vector $\mathbf{z}$.

3.3 Approximation

Now, it is found that the computational complexity is due mainly to the covariance matrix inversion $\mathbf{X}^{-1}$ in our proposed CHATUE-SC-FDMA systems, as indicated by Eqs. (15)–(17). Notice that it can be divided into the covariance matrices of residual ICI, noise, and IBI (past and future) components. The traditional FD-SC/MMSE can exploit the circulant matrix property for the ICI part, by using $\mathbf{F}\mathbf{\Lambda}\mathbf{F}^H \approx \frac{1}{K}\mathrm{tr}[\mathbf{\Lambda}]\mathbf{I}_K$ [11] to approximate it by a diagonal matrix. As shown in Fig. 4, since the central part of residual IBI contains the most important information, it is reasonable that we also use the diagonal approximation for the IBI part as well. Now that $\mathbf{X}^{-1}$ can be approximated by a diagonal matrix, no heavy computation for matrix inversion is needed in our proposed CHATUE-SC-FDMA algorithm in practice.

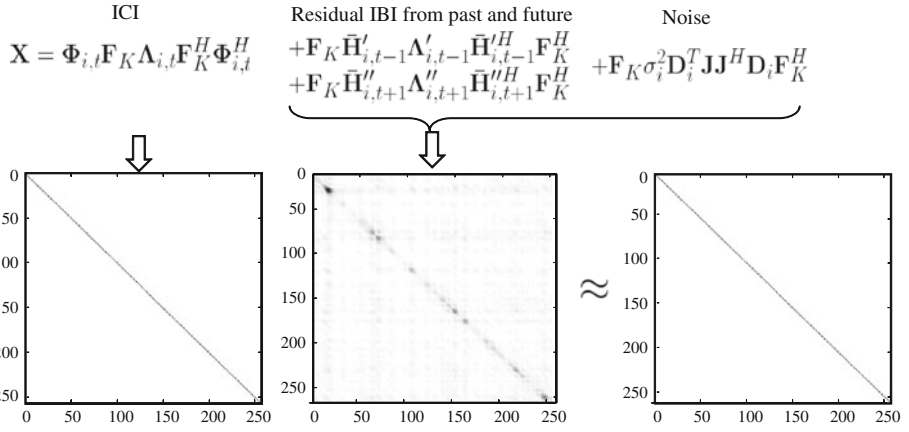

Fig. 4 Shape of covariance matrices, at mutual information of the current, the past and the future to 0.6

Table 1 Computational complexity of CP-SC-FDMA, CHATUE-SC-FDMA with/without DA and CP compensation

Complex operations	CP	CHATUE	CP compensation
Addition	$8K^2$	$14K^2+5K$	$(6+K)K^2+3K$
Multiplication	$14K^2-2K$	$20K^2+2K$	$(7+K)K^2+4K$
Division	K^2	K^2	K^2+K

Finally, $\mathbf{X}$ can be expressed as

$$\begin{aligned}\mathbf{X} &\approx \boldsymbol{\Phi}_{i,t}\boldsymbol{\Lambda}_{i,t}\boldsymbol{\Phi}_{i,t}^H + \operatorname{diag}\Big(\mathbf{F}_K\sigma_i^2\mathbf{D}_i^T\mathbf{J}\mathbf{J}^H\mathbf{D}_i\mathbf{F}_K^H + \mathbf{F}_K\bar{\mathbf{H}}'_{i,t-1}\boldsymbol{\Lambda}'_{i,t-1}\bar{\mathbf{H}}'^H_{i,t-1}\mathbf{F}_K^H \\ &\quad + \mathbf{F}_K\bar{\mathbf{H}}''_{i,t+1}\boldsymbol{\Lambda}''_{i,t+1}\bar{\mathbf{H}}''^H_{i,t+1}\mathbf{F}_K^H\Big) \\ &\approx \boldsymbol{\Phi}_{i,t}\boldsymbol{\Lambda}_{i,t}\boldsymbol{\Phi}_{i,t}^H + \frac{1}{K}\operatorname{tr}\left[\sigma_i^2\mathbf{D}_i^T\mathbf{J}\mathbf{J}^H\mathbf{D}_i + \bar{\mathbf{H}}'_{i,t-1}\boldsymbol{\Lambda}'_{i,t-1}\bar{\mathbf{H}}'^H_{i,t-1} + \bar{\mathbf{H}}''_{i,t+1}\boldsymbol{\Lambda}''_{i,t+1}\bar{\mathbf{H}}''^H_{i,t+1}\right]\mathbf{I}_K\end{aligned} \tag{23}$$

3.4 Complexity Analysis

Without the approximation presented in Sect. 3.3, the matrix inversion $\mathbf{X}^{-1}$ in Eqs. (15)–(17) obviously dominates the computational complexity of our proposed scheme. However, with the approximation presented in Sect. 3.3, it imposes no longer unacceptable computational complexity. A quantitative comparison of the overall computational complexity is provided in Table 1.[1] It is found from Table 1 that the both CP-SC-FDMA and CHATUE-SC-FDMA require the same order of complexity $O(K^2)$ (per iteration). We also evaluated the computational complexity with another CP-free technique, which is not for SC-FDMA but for single-carrier signaling, CP compensation technique presented in [10], and found that it requires complexity of $O(K^3)$, as shown in Table 1. Therefore, it can be concluded that the CHATUE-SC-FDMA algorithm can eliminate IBI without imposing unacceptably higher computational complexity over the traditional CP-SC-FDMA.

4 EXIT Analysis

Extrinsic Transfer Information (EXIT) chart is used to analyze convergence property of the turbo equalizer. In this Section we investigate the effects of providing LLR from the past and future blocks as well as using DA. The mutual information (MI) between LLR and the transmitted bit S is given by

$$\mathrm{MI}_{i,t} = \frac{1}{2}\sum_{s=+1,-1}\int_{-\infty}^{\infty} p_i(\varepsilon|S=s)\log_2\left[\frac{2p_i(\varepsilon|S=s)}{p_i(\varepsilon|S=-1)+p_i(\varepsilon|S=+1)}\right]d\varepsilon. \tag{24}$$

Equation (24) can be evaluated by measuring the histogram of the probabilities $p_i(\varepsilon|S=\pm 1)$, and using some numerical integration technique.

To analyze the impact of the use of the *a posteriori* LLR feedback from the future and the past, we conducted EXIT analysis in an exemplifying system scenario. In the simulation, it was assumed that the number of sub-carriers is $M=512$ and the length of CP is $M/8=64$.

[1] Computational steps for DFT and IDFT are not included in Table 1.

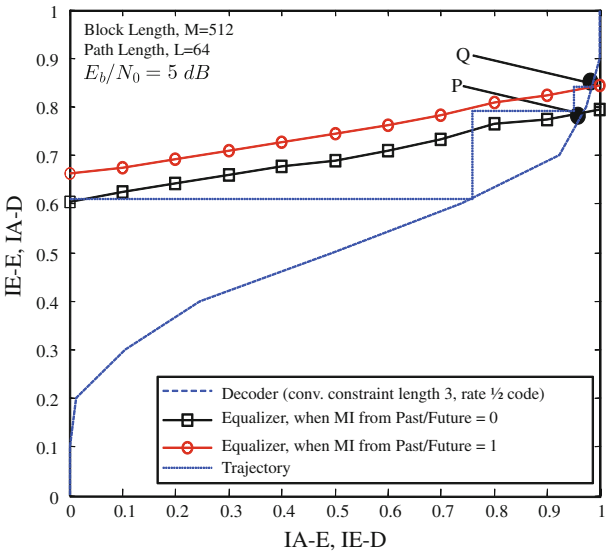

Fig. 5 EXIT chart of CHATUE-SC-FDMA at $E_b/N_0 = 5$ dB without DA for user 1, where IA-E and IE-D indicate the *a priori* mutual information for the equalizer and the extrinsic mutual information for the decoder, respectively. IE-E and IA-D denote the extrinsic mutual information for the equalizer, and the *a priori* mutual information for the decoder, respectively

The number of users is $I = 2$ and $K = 256$ sub-carriers were mapped to each user. BPSK and distributed sub-carrier mapping scheme were used. A rate 1/2 memory 2 nonsystematic recursive convolutional code (RSRCC) encoder was used, and DA's doping rate $p = 8$ was assumed. The decoder for DA, denoted by DA^{-1}, utilized the traditional Bahl–Cocke–Jelink–Raviv (BCJR) [12] algorithm. Each channel path was generated using Jakes' model, and block fading was assumed. By setting the MI from the $(t-2)$th and $(t+2)$th blocks at zero, we can keep the low latency (i.e, truncation length $= 3$). We used the EXIT projection technique because $I = 2$. i.e, when evaluating the MI exchange of the 1st user, given the *a priori* mutual information $\mathrm{MI}_{1,t}$, the 2nd user performs iterations as many times as no more increase in MI is achieved for the equalizer-decoder loops with $t = -1, 0, 1$.

Figure 5 shows the lower bound and the upper bound of the EXIT curves obtained, respectively, where MI from the past and the future is equal to zero, corresponding to the case where IBI components are not cancelled at all, and MI from past and future equal to one, corresponding to the case where IBI can be completely cancelled. It is found from the figure that providing LLR from the neighboring blocks lifts up the equalizer's EXIT curve to avoid the intersection with the decoder's EXIT curve: without the LLR feedback from the neighboring blocks, intersection happens at the point P; with the LLRs feedback, it is lifted up to the point Q; and hence the performance is improved. The trajectory illustrates that at least three iteration are needed in this case.

It is shown in Fig. 6a that by utilizing the DA [13,14], the equalizer's EXIT curve can reach the top-right (1,1) MI point, and furthermore the gap between equalizer and decoder is smaller than the case shown in Fig. 5, and hence the information-rate lose from the capacity can will be reduced [15]. However, it is found from the trajectory that much more iterations are needed than the case of Fig. 5. Figure 6b also shows the corresponding bit error rate (BER) curve. It is found that if the MI from the past and future blocks is equal to one, much

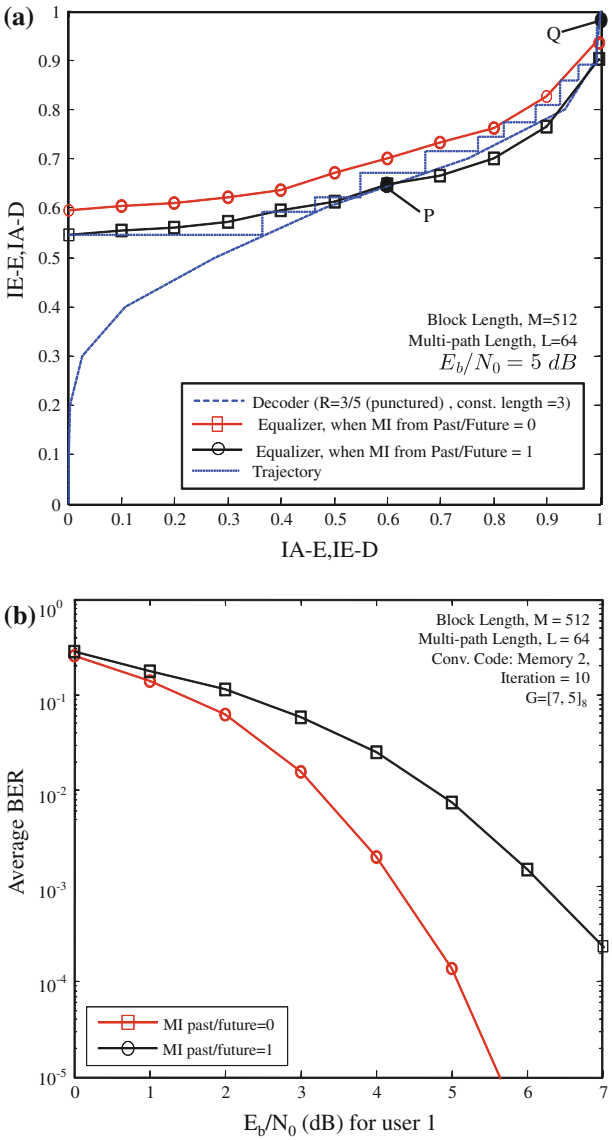

Fig. 6 EXIT chart of CHATUE-SC-FDMA with DA and the corresponding BER performance for user 1

better performance can be achieved than the case when MI from the past and future blocks is equal zero; this observation is consistent to the analysis shown in Fig. 6a.

5 Performance Comparison

5.1 Bit Error Rate Performance

The parameters used in this section are the same as those used in Sect. 4. Note that with the CP transmission, the CP length is assumed to be equal to the multi-path length L. With

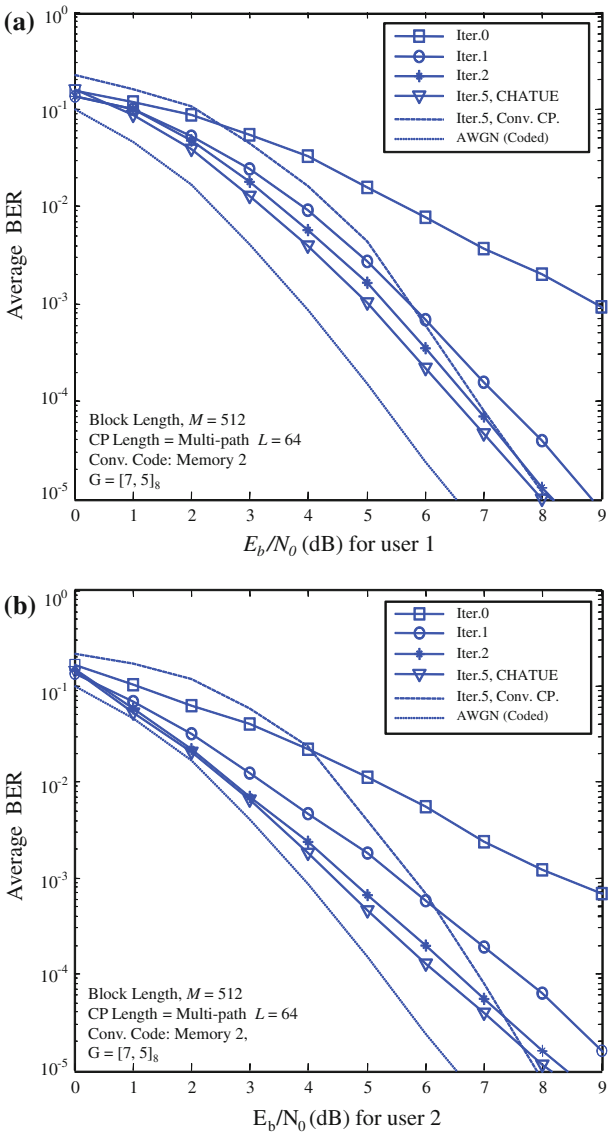

Fig. 7 BER performance of CHATUE for SC-FDMA without DA

CHATUE-SC-FDMA, the vertical LLR exchange to the past and future equalizers is followed by one horizontal iteration between the equalizer and decoder in the current block.

Figure 7a and b show the BER performance with the 1st and the 2st users, respectively, without DA. It is found that CHATUE-SC-FDMA even without DA, CHATUE-SC-FDMA can achieve better performance than traditional CP-SC-FDMA, when $E_b/N_0 < 8$ dB for the both users. It should be noted that with the traditional CP-SC-FDMA system the CP length is 64 and block length is 512 in the simulations. Hence, we can save up to $100 \times L/M$ (CP length / block length) % spectral efficiency.

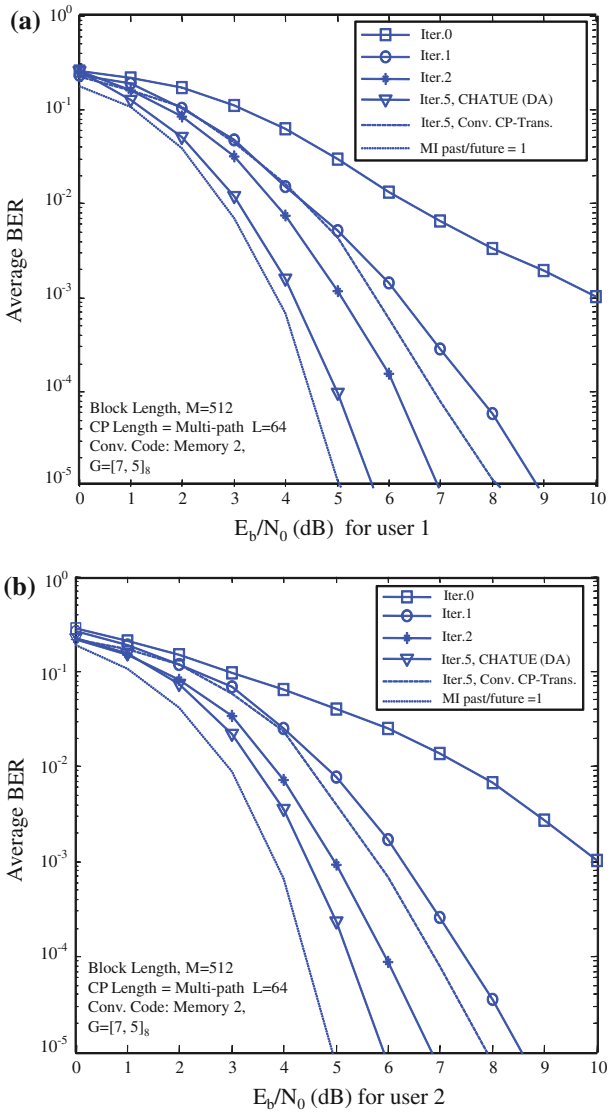

Fig. 8 BER performance of CHATUE for SC-FDMA with DA

Figure 8a and b show with DA the BER curves of the 1st and the 2nd users, respectively. It is found that by utilizing a DA the performance can further be improved by almost 2.5 dB over the traditional CP-SC-FDMA with FD/SC-MMSE equalization.

Since each user is independently transmitted with the non-overlapping sub-carrier allocation, there is no inter-user-interference, and hence the performance should be independent of the number of users. However, as shown in Fig. 9 the BER performance of CHATUE-SC-FDMA degrades as the number of users increases. This is because to keep the orthogonality in sub-carrier mapping, the interlever size for each user has to be smaller when increasing the number of users, and thereby, CHATUE-SC-FDMA turbo equalization can not achieve

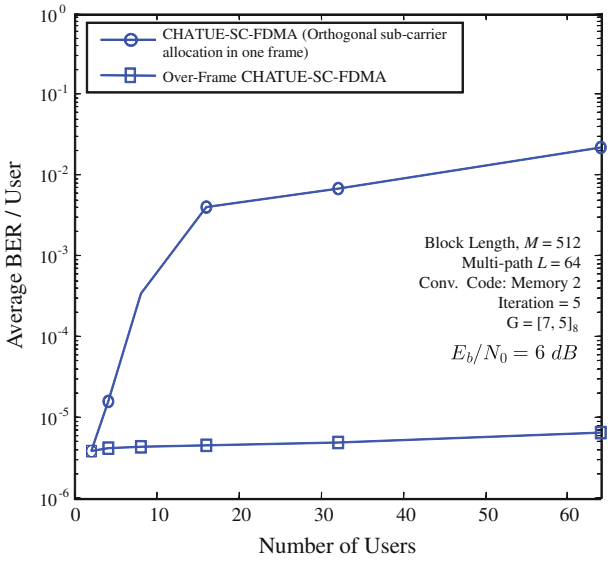

Fig. 9 BER performance with multiple users at $E_b/N_0 = 6\,\text{dB}$

high enough gain through iterations. Figure 9 also shows BER performance achieved by performing over-frame interleving. It is found that the BER performance is not significantly affected, even when the 512 sub-carriers are shared by 64 users. However, detailed considerations on the over-frame interleving technique is out of the scope of this paper. In fact, we have found other relevant advantageous points with the over-frame interleaving technique in the CHATUE framework, which will be reported in another publication.

5.2 Puncturing

It is obvious that for the industry, it is not preferable to change the frame structure specified already by a standard. We also evaluated the performances of traditional CP-SC-FDMA and CHATUE-SC-FDMA with the same block length. We punctured the same memory length code for FD-SC/MMSE with CP, to keep the information bit rate the same as with CHATUE-SC-FDMA, which leads to

$$N \times \frac{1}{R_{cp}} \times \frac{M_{cp}}{K_{cp}} + L = N \times \frac{1}{R_{chatue}} \times \frac{M_{chatue}}{K_{chatue}}, \tag{25}$$

where N denotes the size of information part before encoding. i.e, when $K = 256$ and $M = 512$, the puncturing pattern

$$P = \begin{bmatrix} 1 & 1 & 1 & 0 \\ 1 & 1 & 1 & 1 \end{bmatrix} \tag{26}$$

is used to adjust the information bit rate of the two schemes.

The beneficial point of CHATUE-SC-FDMA is that we can use lower rate coding (strong code) by utilizing the time duration made available by not having to transmit CP. As shown in Fig. 10, CHATUE-SC-FDMA can yield better performance than CP-SC-FDMA while keeping the same information rate. Combined use of CHATUE-SC-FDMA with DA can be

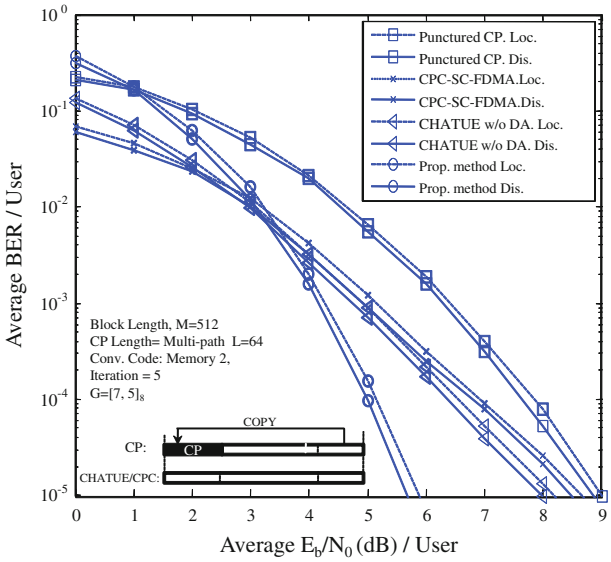

Fig. 10 BER performance of CHATUE for SC-FDMA, traditional SC-FDMA punctured with identical block length and CP compensation

achieved around 3.5 dB better BER performance than punctured traditional CP-SC-FDMA with FD/SC-MMSE equalization. Figure 10 also shows BER performances with distributed and localized sub-carrier allocations. It is found that the performances are almost the same.

We also made performance comparison between the CHATUE-SC-FDMA technique and the CP-compensation technique presented in [10] for single-carrier signaling through computer simulations. We first modified the algorithm presented in [10] such that it can also be suited for SC-FDMA (the modified algorithm is referred to as CPC-SC-FDMA in this paper), and then evaluated its BER performance under the same parameter setting as that used in CHATUE-SC-FDMA. Figure 10 also shows BER curves of CPC-SC-FDMA with distributed and localized sub-carrier allocations. It is found that CHATUE-SC-FDMA without DA can achieve 0.5 dB better performance than CPC-SC-FDMA in a BER range of $10^{-4} - 10^{-5}$; with DA, proposed CHATUE-SC-FDMA achieves roughly 3 dB better performance than CPC-SC-FDMA. It should be emphasized here that as described in Sect. 3.4, the computational complexity required by the CHATUE algorithm is of $O(K^2)$ while that by CPC is of $O(K^3)$. Hence, it can be concluded that the proposed CHATUE-SC-FDMA technique outperforms that presented in [10], while reducing the complexity.

6 Conclusions

This paper has applied the CHATUE concept, presented in the part-1 paper of this article, to SC-FDMA, for which significant modifications were made on the original CHATUE algorithm. It has been shown that the CHATUE algorithm, combined with the doped accumulator, can achieve excellent ICI and IBI cancellation performances for multi-user SC-FDMA systems. By utilizing the structure of the residual covariances where diagonal elements dominate the matrix, an approximation technique is proposed. With the approximation, the necessity for the matrix inversion can be avoided, and hence the computational complexity is

significantly low. Our proposed CHATUE-SC-FDMA systems can achieve $100 \times L/M$ (CP length / block length) % improvement in higher spectral efficiency compared to traditional CP-SC-FDMA with FD/SC-MMSE equalization. On the other hand, if number of the information bits per block has to be kept identical (CHATUE-SC-FDMA has the same spectral efficiency as CP-SC-FDMA), CHATUE-SC-FDMA can use even lower rate code for error protection than CP-SC-FDMA by utilizing the time duration made available by not having to transmit CP. In this case CHATUE-SC-FDMA can achieve better BER performance than CP-SC-FDMA, and hence the power efficiency can be improved.

Appendix: Signal Model and MMSE Algorithm for CHATUE-SC-FDMA

At the transmitter, as shown in Fig. 1, information bits to be transmitted is encoded by the encoder $\mathbf{C}_{i,t}$, interleaved by random interleaver $\mathbf{\Pi}_{i,t}$, doped-Accumulated and modulated to obtain the signal vector $\mathbf{s}_{i,t}$ at the symbol index t (current) for ith user, which is denoted by

$$\mathbf{s}_{i,t} = \left[s(0)_{i,t}, s(1)_{i,t}, \ldots, s(K-1)_{i,t}\right]^T \in C^{K\times 1} \tag{27}$$

The transmitted signal at the block index $t-1$ (past) is given by

$$\mathbf{s}'_{i,t-1} = \left[0, \ldots, 0, s(K-L+1)_{i,t-1}, \ldots, s(K-1)_{i,t-1}\right]^T \in C^{K\times 1}, \tag{28}$$

and that at the block index $t+1$ (future) by

$$\mathbf{s}''_{i,t+1} = \left[s(0)_{i,t+1}, \ldots, s(L-2)_{i,t+1}, 0, \ldots, 0\right]^T \in C^{K\times 1}. \tag{29}$$

With CHATUE, CP transmission is not used, for which the channel matrix for the current block has a Toeplitz structure, as

$$\mathbf{H}_{i,t} = \begin{bmatrix} h(0)_{i,t} & & & 0 \\ \vdots & h(0)_{i,t} & & \\ h(L-1)_{i,t} & \vdots & \ddots & \\ & h(L-1)_{i,t} & \vdots & h(0)_{i,t} \\ & & \ddots & \vdots \\ 0 & & & h(L-1)_{i,t} \end{bmatrix} \in C^{(K+L-1)\times K}, \tag{30}$$

while the channel matrix for the interference components from the past block is

$$\mathbf{H}'_{i,t-1} = \begin{bmatrix} h(L-1)_{i,t-1} & \cdots & h(1)_{i,t-1} \\ & \ddots & \vdots \\ & & h(L-1)_{i,t-1} \\ 0 & & \end{bmatrix} \in C^{(K+L-1)\times K}, \tag{31}$$

and from future block is

$$\mathbf{H}''_{i,t+1} = \begin{bmatrix} & & 0 \\ h(0)_{i,t+1} & & \\ \vdots & \ddots & \\ h(L-2)_{i,t+1} & \cdots & h(L-2)_{i,t+1} \end{bmatrix} \in C^{(K+L-1)\times K}. \tag{32}$$

Toeplitz structure of $\mathbf{H}_{i,t}$ of Eq. (30) can be converted to curculant structure by multiplying the $\mathbf{J}$ matrix given by

$$\mathbf{J} = \begin{bmatrix} & & 1 & & 0 \\ & & & 1 & \\ 1 & & & & 1 \\ & \ddots & & & \ddots \\ 0 & & 1 & & & 1 \end{bmatrix} \in C^{K\times(K+L-1)}, \tag{33}$$

as explained in the sentence before Eq. (1).

MMSE weight is given by

$$\mathbf{w}_{i,t}(k) = \arg\min_{\mathbf{w}_{i,t}^H(k)} \left|\mathbf{w}_{i,t}^H(k)\tilde{s}_{i,t}(k) - s_{i,t}(k)\right|^2. \tag{34}$$

To obtain the solution to this optimization problem, we need to solve

$$\mathrm{E}\left[\frac{\partial}{\partial \mathbf{w}_{i,t}^H(k)}\left|\mathbf{w}_{i,t}^H\tilde{s}(k)_{i,t} - s_{i,t}(k)\right|\right] = 0, \tag{35}$$

where $\tilde{s}(k)_{i,t}$ is given by Eq. (14). By taking partial derivative, we obtain

$$\begin{aligned}\mathbf{w}_{i,t}(k) &= \mathrm{E}[|\tilde{\mathbf{r}}_{i,t} + \bar{h}_{i,t}(k)\tilde{s}_{i,t}(k)|]^2)^{-1}\mathrm{E}[(\tilde{\mathbf{r}}_{i,t} + \bar{h}_{i,t}(k)\tilde{s}_{i,t}(k))\tilde{\mathbf{s}}_{i,t}^*(k)] \\ &= \Big(\bar{\mathbf{H}}_{i,t}\mathbf{\Lambda}_{i,t}\bar{\mathbf{H}}_{i,t}^H + \sigma_i^2\mathbf{D}_i^T\mathbf{J}\mathbf{J}^H\mathbf{D}_i + \bar{\mathbf{H}}'_{i,t-1}\mathbf{\Lambda}'_{i,t}\bar{\mathbf{H}}'^H_{i,t-1} + \bar{\mathbf{H}}''_{i,t+1}\mathbf{\Lambda}''_{i,t}\bar{\mathbf{H}}''^H_{i,t+1} \\ &\quad + \bar{\mathbf{h}}_{i,t}(k)|\mathbf{s}_{i,t}(k)|^2\bar{\mathbf{h}}_{i,t}^H(k)\Big)^{-1}\bar{\mathbf{h}}_{i,t}(k) \\ &= \left(\mathbf{\Sigma}_{i,t} + \bar{h}_{i,t}(k)|\mathbf{s}_{i,t}(k)|^2\bar{h}_{i,t}^H(k)\right)^{-1}\bar{h}_{i,t}(k),\end{aligned} \tag{36}$$

where the modulation-level covariance matrix is given by

$$\mathbf{\Lambda}_{i,t} = \mathrm{diag}\left\{\mathrm{E}[|\hat{\mathbf{s}}_{i,t}|^2] - |\hat{\mathbf{s}}_{i,t}|^2\right\}. \tag{37}$$

The output of FD/SC-MMSE $z(k)_{i,t}$ can be expressed as

$$\begin{aligned}z(k)_{i,t} &= \mathbf{w}_{i,t}^H(k)\tilde{s}_{i,t}(k) = \mathbf{w}_{i,t}^H(k)(\tilde{\mathbf{r}}_{i,t} + \mathbf{h}_{i,t}(k)\hat{\mathbf{s}}_{i,t}(k)) \\ &= (1+\gamma(k)|\hat{s}_{i,t}(k)|^2)^{-1}\mathbf{h}_{i,t}^H(k)\mathbf{\Sigma}_{i,t}^{-1}\cdot(\tilde{\mathbf{r}}_{i,t}(k) + \mathbf{h}_{i,t}(k)\hat{\mathbf{s}}_{i,t}(k)),\end{aligned} \tag{38}$$

where

$$\gamma(k) = \mathbf{h}_{i,t}^H(k)\mathbf{\Sigma}_{i,t}^{-1}\mathbf{h}_{i,t}(k) \tag{39}$$

with

$$\mathbf{\Sigma}_{i,t} = \bar{\mathbf{H}}_{i,t}\mathbf{\Lambda}_{i,t}\bar{\mathbf{H}}_i, t^H + \bar{\mathbf{H}}'_{i,t-1}\mathbf{\Lambda}'_{i,t-1}\bar{\mathbf{H}}'^H_{i,t-1} + \bar{\mathbf{H}}''_{i,t+1}\mathbf{\Lambda}''_{i,t+1}\bar{\mathbf{H}}''^H_{i,t+1} + \sigma_i^2\mathbf{D}_i^T\mathbf{J}\mathbf{J}^H\mathbf{D}_i. \tag{40}$$

By sorting $z_{i,t}(k)$ over k into a vector $\mathbf{z}_{i,t}$, we have the block-wise expression

$$\mathbf{z}_{i,t} = (\mathbf{I}_k + \mathbf{\Gamma}_{i,t}\mathbf{S}_{i,t})^{-1}\left[\mathbf{\Gamma}_{i,t}\hat{\mathbf{s}}_{i,t} + \bar{\mathbf{H}}_{i,t}^H\mathbf{\Sigma}_{i,t}^{-1}\tilde{\mathbf{r}}_{i,t}\right]. \tag{41}$$

Now, recall Eq. (13), we have

$$\begin{aligned}\mathbf{z}_{i,t} &= (\mathbf{I}_k + \mathbf{\Gamma}_{i,t}\mathbf{S}_{i,t})^{-1}\left[\mathbf{\Gamma}_{i,t}\hat{\mathbf{s}}_{i,t} + \mathbf{F}_K^H \mathbf{\Phi}^H \mathbf{F}_K \mathbf{\Sigma}_{i,t}^{-1}\tilde{\mathbf{r}}_{i,t}\right] \\ &= (\mathbf{I}_k + \mathbf{\Gamma}_{i,t}\mathbf{S}_{i,t})^{-1}\left[\mathbf{\Gamma}_{i,t}\hat{\mathbf{s}}_{i,t} + \mathbf{F}_K^H \mathbf{\Phi}^H \mathbf{X}^{-1}\mathbf{F}_K\tilde{\mathbf{r}}_{i,t}\right] \end{aligned} \tag{42}$$

with

$$\mathbf{S}_{i,t} = \mathrm{diag}\left(\left|\hat{\mathbf{s}}_t^2\right|\right). \tag{43}$$

References

1. Tanno, M., Kishiyama, Y., Higuchi, K., & Sawahashi, M. (2007). Evolved UTRA-physical layer overview. *SPAWC* (pp. 1–8).
2. Myung, H., & Goodman, D. J. (1996). Single carrier FDMA for uplink wireless transmission. *IEEE Vehicle Technology. Mag, 1*.
3. Anwar, K., & Matsumoto, T. (2011). Low complexity time-concatenated turbo equalization for block transmission without guard interval: Part 1—the concept. *Wireless Personal Communications*, Springer, Submitted.
4. Huang, G., Nix, A., & Armour, S. (2008). Decision feedback equalization in SC-FDMA. In *19th International Symposium on Personal, Indoor and Mobile Radio Communications* (pp. 1–5).
5. Zhang, C., Wang, Z., Yang, Z., Wang, J., & Song, J. (2010). Frequency domain decision feedback equalization for uplink SC-FDMA. *IEEE Transactions on Broadcasting, 56*, 253–257.
6. Wang, Z., Ma, X., & Giannakis, G. B. (2004). OFDM or single-carrier block transmissions? *IEEE Transactions on Communications, 52,* 380–394.
7. Zhou, H., Anwar, K., & Matsumoto, T. (2010). Chained turbo equalization for SC-FDMA systems without cyclic prefix. In *IEEE Globecom 2010 Workshop on Broadband Single Carrier and Frequency Domain Communications*.
8. Liu, C. Y., Chen, Y. F., & Li, C. P. (2009). Blind beamforming schemes in SC-FDMA systems with insuffient cyclic prefix and carrier frequency offset. *IEEE Transactions on Vehicular Technology, 58*, 4848–4858.
9. Kansanen, K., & Matsumoto, T. (2003). A computationally effient MIMO turbo equalizer. In *IEEE VTC-Spring, Korea, 1* (pp. 277–281).
10. Lee, H., Lee, Y., & Park, H. (2011). An efficient CP compensation for SC-FDE with insufficient CP symbols. *IEEE Communication Letters, 14*, 548–550.
11. Kansanen, K., & Matsumoto, T. (2007). An analytical method for MMSE MIMO turbo equalizer EXIT chart computation. *IEEE Transactions on Communications, 6*, 59–63.
12. Bahl, L., Cocke, J., Jelinek, F., & Raviv, J. (1974). Optimal decoding of linear codes for minimizing symbol error rate. *IEEE Transactions on Information Theory, 20*, 284–287.
13. ten Brink, S. (2000). Rate one-half code for approaching the Shannon limit by 0.1 dB. *IEEE Electron Letters, 36*, 1293–1294.
14. Pfletschinger, S., & Sanzi, F. (2006). Error floor removal for bit-interleaved coded modulation with iterative detection. *IEEE Transactions on Wireless Communications, 5*, 3174–3181.
15. Asikmin, A., Kramer, G., & Brink, S. (2004). Extrinsic information transfer functions: Model and erasure channel properties. *IEEE Transactions on Information Theory, 50,* 2657–2673.

Author Biographies

Hui Zhou received BS degree from the school of electrical engineering and automation, Henan Polytechnic University (HPU), China in 2006. He was a research student in the school of Information Science, Nara Institute of Science and Technology (NAIST) until 2008. He received MS degree from the school of Information Science, Japan Advanced Institute of Science and Technology (JAIST) in 2010. Now he is a PhD student in Information Theory and Signal Processing Laboratory in JAIST. He received Young Researcher's Encouragement Award from IEEE VTS Japan in 2010. His research interests are channel estimation, interference cancellation and channel dependent scheduling for LTE.

Khoirul Anwar graduated (*cum laude*) from the department of Electrical Engineering (Telecommunications), Institut Teknologi Bandung (ITB), Bandung, Indonesia in 2000. He received Master and Doctor Degrees from Graduate School of Information Science, Nara Institute of Science and Technology (NAIST) in 2005 and 2008, respectively. Since then, he has been appointed as an assistant professor in NAIST. He received best student paper award from the IEEE Radio and Wireless Symposium 2006 (RWS'06), California-USA, and Best Paper of Indonesian Student Association (ISA 2007), Kyoto, Japan in 2007. Since September 2008, he is with the School of Information Science, Japan Advanced Institute of Science and Technology (JAIST) as an assistant professor. His research interests are network information theory, error control coding, iterative decoding and signal processing for wireless communications. He has authored around 45 scientific publications in these areas. He serves as a reviewer for a number of main journals and conferences in the area of wireless communications and signal processing. Dr. Anwar is a member of IEEE, information theory society, and IEICE Japan.

Tad Matsumoto received his BS, MS, and PhD degrees from Keio University, Yokohama, Japan, in 1978, 1980, and 1991, respectively, all in electrical engineering. He joined Nippon Telegraph and Telephone Corporation (NTT) in April 1980. Since he engaged in NTT, he was involved in a lot of research and development projects, all for mobile wireless communications systems. In July 1992, he transferred to NTT DoCoMo, where he researched Code-Division Multiple-Access techniques for Mobile Communication Systems. In April 1994, he transferred to NTT America, where he served as a Senior Technical Advisor of a joint project between NTT and NEXTEL Communications. In March 1996, he returned to NTT DoCoMo, where he served as a Head of the Radio Signal Processing Laboratory until August of 2001; He worked on adaptive signal processing, multiple-input multiple-output turbo signal detection, interference cancellation, and space-time coding techniques for broadband mobile communications. In March 2002, he moved to University of Oulu, Finland, where he served as a Professor at Centre for Wireless Communications. In 2006, he served as a Visiting Professor at Ilmenau University of Technology, Ilmenau, Germany, funded by the German MERCATOR Visiting Professorship Program. Since April 2007, he has been serving as a Professor at Japan Advanced Institute of Science and Technology (JAIST), Japan, while also keeping the position at University of Oulu. Prof. Matsumoto has been appointed as a Finland Distinguished Professor for a period from January 2008 to

December 2012, funded by the Finnish National Technology Agency (Tekes) and Finnish Academy, under which he preserves the rights to participate in and apply to European and Finnish national projects. Prof. Matsumoto is a recipient of IEEE VTS Outstanding Service Award (2001), Nokia Foundation Visiting Fellow Scholarship Award (2002), IEEE Japan Council Award for Distinguished Service to the Society (2006), IEEE Vehicular Technology Society James R. Evans Avant Garde Award (2006), and Thuringen State Research Award for Advanced Applied Science (2006), 2007 Best Paper Award of Institute of Electrical, Communication, and Information Engineers of Japan (2008), Telecom System Technology Award by the Telecommunications Advancement Foundation (2009), and IEEE Communication Letters Exemplifying Reviewer Award (2011). He is a Fellow of IEEE and a Member of IEICE. He is serving as an IEEE Vehicular Technology Distinguished Lecturer during the term July 2011–June 2013.